Published OnlineFirst February 26, 2018; DOI: 10.1158/1535-7163.MCT-17-0827

Models and Technologies

Molecular Cancer Therapeutics

Anti-HER2 scFv-Directed Extracellular Vesicle-Mediated mRNA-Based Gene Delivery Inhibits Growth of HER2-Positive Human Breast Tumor Xenografts by Prodrug Activation

Jing-Hung Wang[1], Alexis V. Forterre[1], Jinjing Zhao[1], Daniel O. Frimannsson[1], Alain Delcayre[2], Travis J. Antes[3], Bradley Efron[4], Stefanie S. Jeffrey[5], Mark D. Pegram[6], and A.C. Matin[1]

Abstract

This paper deals with specific targeting of the prodrug/enzyme regimen, CNOB/HChrR6, to treat a serious disease, namely HER2$^+$ human breast cancer with minimal off-target toxicity. HChrR6 is an improved bacterial enzyme that converts CNOB into the cytotoxic drug MCHB. Extracellular vesicles (EV) were used for mRNA-based H*chrR6* gene delivery: EVs may cause minimal immune rejection, and mRNA may be superior to DNA for gene delivery. To confine HChrR6 generation and CNOB activation to the cancer, the EVHB chimeric protein was constructed. It contains high-affinity anti-HER2 scFv antibody (ML39) and is capable of latching on to EV surface. Cells transfected with EVHB-encoding plasmid generated EVs displaying this protein ("directed EVs"). Transfection of a separate batch of cells with the new plasmid, XPort/HChrR6, generated EVs containing HChrR6 mRNA; incubation with pure EVHB enabled these to target the HER2 receptor, generating "EXO-DEPT" EVs. EXO-DEPT treatment specifically enabled HER2-overexpressing BT474 cells to convert CNOB into MCHB in actinomycin D–independent manner, showing successful and specific delivery of HChrR6 mRNA. EXO-DEPTs—but not undirected EVs—plus CNOB caused near-complete growth arrest of orthotopic BT474 xenografts *in vivo*, demonstrating for the first time EV-mediated delivery of functional exogenous mRNA to tumors. EXO-DEPTs may be generated from patients' own dendritic cells to evade immune rejection, and without plasmids and their potentially harmful genetic material, raising the prospect of clinical use of this regimen. This approach can be used to treat any disease overexpressing a specific marker.
Mol Cancer Ther; 17(5); 1133–42. ©2018 AACR.

Introduction

Chemotherapy is widely used in cancer treatment, but conventional approaches may lack selectivity for tumors versus normal tissues. The result can be insufficient drug concentration in tumors, leading to resistance development and severe side effects. Gene-delivered enzyme prodrug therapy (GDEPT) can potentially ameliorate these problems (1, 2). In this approach, a compound is used that is inert to native human enzymes and is harmless, but upon activation by an enzyme encoded by viral or bacterial gene, is converted into a cytotoxic drug. Provided that the targeting of the gene is specific to tumors, this therapy can confine the drug to the tumor at a high concentration and mitigate off-target effects.

This paper reports specific targeting of the GDEPT regimen we previously described, namely, 6-chloro-9-nitro-5-oxo-5H-benzo-(a)-phenoxazine (CNOB)/HChrR6 to HER2-overexpressing breast cancer. HChrR6 is an *Escherichia coli* enzyme that we discovered, improved, and humanized (refs. 3–6; GenBank accession no. MG838738); it converts CNOB into the cytotoxic drug, 9-p amino-6-chloro-5H-benzo[a]phenoxazine-5-one (MCHB). The latter is strongly fluorescent, can be imaged in living mice, and quantitated by its fluorescence intensity (7). MCHB causes DNA intercalation (3) and is thus likely to kill both growing and nongrowing cells, which is advantageous, as a significant portion of tumor cells is typically quiescent. It has an impressive bystander effect (BE)—BE refers to the leakage of the cytotoxic drug from the transfected tumor cells that also kills the neighboring nontransfected cells and is critical for the effectiveness of GDEPT, as no method of gene delivery can transfect all the cells in a tumor.

To determine the *in vivo* efficacy of this regimen in these initial studies, we had avoided the issue of specific targeting by using 4T1 murine mammary cells that endogenously generated HChrR6 enzyme to implant tumors in mice; marked improvement was seen in the survival of mice treated with CNOB (3, 8). To now develop a targeting strategy, we have chosen HER2$^+$ breast cancer. This disease is associated with poor prognosis. HER2 is part of

[1]Department of Microbiology and Immunology, Stanford University School of Medicine, Stanford, California. [2]ExoThera LLC, Menlo Park, California. [3]Systems Biosciences, Palo Alto, California. [4]Department of Statistics, Stanford University, Stanford, California. [5]Department of Surgery, Stanford University School of Medicine, Stanford, California. [6]Department of Medicine, Stanford University School of Medicine, Stanford, California.

Note: Supplementary data for this article are available at Molecular Cancer Therapeutics Online (http://mct.aacrjournals.org/).

Current address for J. Zhao: First Affiliated Hospital of Guangzhou Medical University, Guangzhou, P.R. China; current address for D.O. Frimannsson: Bristol-Myers Squibb, Redwood City, California; and current address for T.J. Antes: Cedars-Sinai Heart Institute, Los Angeles, California.

Corresponding Author: A.C. Matin, Stanford University School of Medicine, 299 Campus Drive West, Stanford, CA 94305-5124. Phone: 650-725-4745; Fax: 650-725-6757; E-mail: a.matin@stanford.edu

doi: 10.1158/1535-7163.MCT-17-0827

Published OnlineFirst February 26, 2018; DOI: 10.1158/1535-7163.MCT-17-0827

the type 1 receptor tyrosine kinase signaling network; dysregulation of this network by HER2 gene amplification results in cancer (9–13). The marked increase in the HER2 receptor has been exploited to design targeted therapies, e.g., trastuzumab and lapatinib, for treating this disease (13–17). The same feature made it an attractive model system for us to design the above-mentioned new treatment for this cancer. New approaches to treat this cancer are needed, as the trastuzumab type of drugs, while effective, can be hampered by resistance development and side effects.

Viruses have commonly been used for gene delivery in GDEPTs, but raise concerns of immune recognition, insertional mutagenesis, and inflammatory toxicity (18). We have used extracellular vesicles (EV, also called exosomes) instead. These are small, consist of lipid bilayers, are constitutively generated by most body cells, are largely nontoxic, and are able to deliver their cargo directly into the cytoplasm. They can also avoid the endosomal pathway and lysosomal degradation, as discussed below. Their small size mitigates uptake by the reticuloendothelial system and permits extravasation through vessel fenestrations present in tumors. Being means of intracellular communication, they may be minimally immunogenic, especially when derived from mesenchymal stem cells (19) or from patient's own, e.g., dendritic cells (20–25).

Herpes simplex virus type 1 thymidine kinase and ganciclovir (HSV-tk/GCV) GDEPT has been tested in a phase III clinical trial for treating glioblastoma multiforme patients (26). No beneficial results were seen, in which low-level and short-lived gene expression had an important role (27); this factor has also contributed to the failure of additional prodrug regimens to proceed beyond phase I/II stages (28, 29). A possible reason for poor gene expression might be the use of DNA for gene delivery as, to be effective, DNA must be transported into the nucleus. This is a highly inefficient process, as <0.01% to 0.10% cytosolic DNA enters the nucleus (30, 31). We have used mRNA instead as, upon transfer to cytosol, it is directly translated, and eliminates the risk of insertional mutagenesis. Indeed, mRNA- instead of DNA-based gene delivery was more effective in retarding tumor growth (31, 32).

Here, we show that EVs, directed to the HER2 receptor and loaded with HChrR6-encoding mRNA ("EXO-DEPTs"), used in conjunction with CNOB, specifically kill $HER2^+$ cells and cause near-complete growth arrest of implanted orthotopic $HER2^+$ breast cancer tumors in mice. This is the first time that EVs have been successfully used to deliver exogenous functional mRNA to recipient cells and tumors. We note that the approach described here is generic and can be used to treat any disease in which a marker is overexpressed.

Materials and Methods

Cell lines and cell viability

MCF7, MCF7/ErbB2, BT474, BT474/HER-Res, SKBR3, immortalized human kidney embryonic (HEK293) cell lines were used. All were purchased between 2005 and 2009 from ATCC, except 293FT, which was purchased from Thermo Fisher Scientific. Authentication was done in December 2017 by Genetic Resources Core Facility at Johns Hopkins, using short tandem repeat markers. Cells were cultured in DMEM medium (Thermo Fisher Scientific) with 10% fetal bovine serum (FBS) and incubated in a moisturized incubator (37°C; 5% CO_2). *Mycoplasma* testing was done in December 2017 (LookOut Mycoplasma PCR Detection Kit, Sigma-Aldrich; and PCR based MycoDtect kit, Greiner Bio-One North America) and showed no contamination of any of the cell lines. Plasmid p6mLSC1C2 used here was originally generated by Delcayre and colleagues (21); it encodes the mouse lactadherin C1–C2 domains that bind to the EV surface and its leader sequence. Plasmid pACgp67B-HER2m, containing the anti-HER2 scFv (ML39) antibody DNA sequence, was supplied by Addgene; ML39 targets the extracellular domain of HER2 receptor (33). Cell viability was determined by the MTT assay (Roche). Cells were used within 20 passages.

EV preparation

This was done as described previously (34). A total of 5×10^6 cells [10-mL DMEM, plus 10% EV-depleted FBS ("DMEM-EDFBS")] were plated in a 100-mm dish and incubated for 4 days. The conditioned medium (containing the EVs) was centrifuged at $600 \times g$ followed by $2000 \times g$ (30 minutes each) to remove cells and apoptotic bodies, respectively. EVs present in the resulting supernatant were isolated by ultra-centrifugation ($100{,}000 \times g$; 1 hour/15 minutes). Pellets were suspended in PBS; protein assay was by a DC kit (Bio-Rad) and the EVs were characterized by NanoSight (NS300; Melvin Instruments), and transmission electron microscopy (TEM; JEOL JEM1400 TEM). EVs were never frozen and were used fresh.

Western blotting

This was performed as before (34), except that β-mercaptoethanol was not used. Primary antibodies used were mouse anti-human CD63 (1:1,000; ab59479; Abcam), mouse anti-human CD81 (1:500; sc-23962; Santa Cruz Biotechnology), rabbit anti-human MFGE8 (1:1,000; ab168733; Abcam), and goat anti-mouse MFGE8 (lactadherin; 1:5,000, AF2805; R&D Systems). Secondary antibodies used were goat anti-mouse IgG (1:2,000; 115-035-166; Jackson ImmunoResearch), goat anti-rabbit IgG (1:2,000; 7074S; Cell Signaling Technology), and donkey anti-goat IgG (1:2,000; Santa Cruz Biotechnology).

HER2-targeting chimeric protein, LS-ML39-C1–C2-His (EVHB), preparation

cDNA sequence of the anti-HER2 scFv antibody, ML39 (Supplementary Fig. S1), contained in the pACgp67B-HER2m plasmid, was inserted into the p6mLSC1C2 plasmid, using the BsmB1 double restriction site to construct pEVC1C2HER. HEK293 cells (5×10^6) were plated in a 100-mm dish containing 10-mL of DMEM-EDFBS and incubated (CO_2 incubator; 37°C; overnight). They were transfected with pEVC1C2HER (7.2-μg) along with polyethylenimine (PEI; 4-day incubation). EVs generated by the transfected cells, which displayed EVHB, were isolated. (EVHB displaying EVs are termed "directed"; those from nontransfected cells, not displaying this protein, are termed "naïve"). Directed EVs were also made by incubating naïve EVs with pure EVHB (2×10^7 EVs; 1 μg EVHB; 15-minute incubation; room temperature).

EVHB was purified (21) by dissolving EVHB-displaying EVs in MLBII solution (50 mmol/L NaPO4 pH8/300 mmol/L NaCl/ 10 mmol/L imidazole/0.5% Tween 20), followed by incubation in equal volume of Ni-NTA resin (2 hours; mild agitation; 4°C). Samples were transferred to a resin-containing column and washed in 5 volumes of MWBI (50 mmol/L NaPO4 pH8/300 mmol/L NaCl/20 mmol/L imidazole/0.05% Tween 20), and then

Published OnlineFirst February 26, 2018; DOI: 10.1158/1535-7163.MCT-17-0827

in 10 volumes of MWBII (50 mmol/L NaPO4 pH8/300 mmol/L NaCl/20 mmol/L imidazole). The protein was eluted in 10 volumes of MEBII (50 mmol/L $NaPO_4$, pH 8/300 mmol/L NaCl/250 mmol/L imidazole) and was concentrated (Pierce protein concentrator; Thermo Fischer Scientific). For exchange to PBS buffer, Zebra spin desalting columns (Thermo Fischer Scientific) were used. Following further concentration (ultra-centrifugal filters; Amicon), the protein was quantified. Its three-dimensional structure was constructed using Phyre2 Protein Homology/analogy Recognition Engine V2.0 in intensive mode (35), followed by identification of the functional domains and their orientations, using Chimera software (UCSF).

Enzyme-linked immunosorbent assay (ELISA)

HER2 extracellular domain (ECD; ACROBiosystems) was dissolved in carbonate buffer (pH 9.6; final concentration, 5 μg/mL). All procedures were performed on a shaker with mild agitation. The ECD solution (100 μL) was used to coat the wells (4°C overnight); they were rinsed thrice with washing buffer (PBS with 0.05% Tween 20) and treated with blocking buffer (PBS with 0.5% BSA; room temperature; 1 hour). After the addition of EVs (2×10^7 per well) and incubation (room temperature; 2 hours), the wells were rinsed thrice with washing buffer. Anti-CD63 antibody (BD Pharmingen; 5 μg/mL in100-μL of blocking buffer) was added, followed by incubation (room temperature; 1 hour). The wells were washed thrice with washing buffer, followed by blocking buffer supplemented with 100-μL of HRP goat anti-mouse IgG (1:5,000) and incubation at room temperature (1 hour). After three additional washes, 100-μL TMB (Sigma-Aldrich) was added to each well (30-minute incubation). The HRP enzymatic reaction was stopped by 1N-HCl (100 μL/well). A_{450} minus the background absorbance (A_{620}) indicated the intensity of the EV binding to the HER2 receptor.

EV binding determination to cells by microscopy and flow cytometry

Binding of directed-EVs [labeled for visualization with CFSE (Thermo Fischer Scientific)] to (essentially) HER2-negative (MCF7; 4.7-ng HER2 receptor/mg) and positive (BT474; 530-ng HER2 receptor/mg; refs. 15, 16) cells was compared. Cells (3×10^4) per well ($n = 3$) were seeded in a black 96-well plate with transparent bottoms (Thermo Fisher Scientific) and exposed to naïve unlabeled-EVs in DMEM/10%FBS overnight to block nonspecific binding. Directed- or naïve EVs were then added to separate groups of wells and incubated in DMEM/EDFBS (6 hours; 37°C), followed by washing in the same medium (to remove unbound EVs), and addition of fresh medium (100-μL). Green fluorescence (GFP filter) and phase contrast images were taken (20× magnification; EVOS FL Cell Imaging System, Thermo Fisher Scientific).

Cell binding was also analyzed by flow cytometry. BT474 cells tended to form clumps and proved unsuitable, so we used the $HER2^+$ SKBR3 cells (HER2 content, 913-ng/mg); MCF7 cells were again used as control. The EVs were labeled with PKH26 dye (Sigma-Aldrich) by suspending them in 1-mL Diluent C (Sigma-Aldrich) containing PKH26 (4 μL); incubation was at room temperature (5 minutes). Addition of 0.5 mL of PBS-2% BSA stopped the labeling. Following harvest, the EVs were resuspended in 1-mL fresh PBS; any remaining unbound dye was removed (Pierce buffer exchange column; Thermo Fisher Scientific). SKBR3 cells were seeded in 6-well plates (1.2×10^6/well) in DMEM/10% FBS and incubated overnight. The medium was replaced with DMEM/EDFBS containing 1.6×10^9 directed-EVs and incubated at 37°C (4 hours). Cells were washed with ice-cold PBS; 0.2 mL/well of cell detaching solution in PBS (Thermo Fisher Scientific) was added to dislodge the cells, which were mixed with 1 mL DMEM/10% FBS. Cells were harvested ($900 \times g$; 4°C; 5 minutes); rinsed in 1-mL FACS buffer (PBS/1% BSA/0.1% NaN_3); washed with 1 mL of acid buffer (0.5 mol/L NaCl; 0.2 mol/L acetic acid, pH 3.0) to remove noninternalized EVs; and treated with Flow Cytometry Fixation Buffer (R&D Systems; 4°C; overnight). The fixed cells were centrifuged ($900 \times g$; 4°C; 5 minutes), resuspended in 1 mL of FACS buffer, and filtered (40-μm cell strainer; BD Biosciences). Aliquots were analyzed by the Scanford FACS analyzer (excitation, 488 nm; emission, 590/20 nm).

Loading EVs with HChrR6 mRNA

We first used electroporation (36). HChrR6 mRNA (1-μg) was suspended with the EVs in Cytomix electroporation buffer (Bio-Rad) and electroporated (100 to 400 V; 125 μF). EVs were isolated with latex beads (Thermo Fisher Scientific), and their mRNA was quantified (qRT-PCR). This approach having proved inadequate (see Results), we developed a novel method to load EVs with HChrR6 mRNA that involved construction of a new plasmid pXPort/HChrR6, utilizing SBI XPort plasmid (SBI). To prepare EVs loaded with mRNA, 5×10^6 293FT cells were transfected with pXPort/HChrR6 plasmid (7.2-μg/100-mm cell culture plate), along with PEI (2.5 × plasmid weight), incubated (CO_2 incubator; 37°C; 4-days), and then harvested. (EVs containing HChrR6 mRNA are termed "loaded" EVs.)

RNA extraction and quantitative RT-PCR

RNA was extracted using the RNeasy Mini Kit (QIAGEN) and quantified by NanoDrop 1000 Spectrophotometer (Thermo Fisher Scientific). cDNA was synthesized from RNA, using M-MuLV reverse transcriptase [Taq RT-PCR kit, New England Biolabs (NEB)]. To remove any remaining RNA, the cDNA was treated with RNase H (NEB). qPCR was performed [Maxima SYBR Green/ROX qPCR Master Mix Kit (Thermo Fisher Scientific) and 7500/7500 Fast Real-Time PCR System (Applied Biosystems], using GAPDH mRNA as an endogenous control. The following primers were used: HChrR6 Forward 5′-GCAGATCCTCGTGTTCCTGGA-3′, HChrR6 Reverse 5′-CCTGGTCAATCACTTCTCCGTTCT-3′, GAPDH Forward 5′-GGGTGTGAACCATGAGAAGT-3′ and GAPDH Reverse 5′-GGCATGGACTGTGGTCATGA-3′. The EV mRNA copy number was estimated employing a standard curve, using the following formula: $[X(\text{ng}) \times 6.0221 \times 10^{23}$ (molecules/mole)]/$[N \times 330$ (g/mole) $\times 10^9$ (ng/g)], where X is the amount of EV mRNA, N is its length, and 330 is the average molecular weight of individual nucleotides (Rhode Island Genomics and Sequencing Center).

In vitro assays for EXO-DEPT EV functionality

BT474 cells suspended in 100-μL DMEM-EDFBS were seeded (3×10^4 per well) in a 96-well plate and incubated (37°C; 4 hours) to allow attachment. EVs (8×10^8) were added to each well, followed by overnight incubation. For treatment with actinomycin D (10 μg/mL) or cycloheximide (1 μmol/L), cells were preincubated in the same medium supplemented with either of these inhibitors (3 hours). The medium was then replaced with 100 μL of phenol red-free DMEM/10% FBS/15 μmol/L CNOB.

Published OnlineFirst February 26, 2018; DOI: 10.1158/1535-7163.MCT-17-0827

After 24-hour incubation, functional activity of the EV-delivered HChrR6 mRNA in target cells was determined by measuring MCHB fluorescence (excitation, 570 nm; emission, 620 nm), using a fluorescence plate reader (SpectraMax, Molecular Devices).

In vivo assays for EXO-DEPT EV functionality

All animal experiments were approved by Stanford University Institutional Animal Care and Use Committee (IACUC). The number of mice required for this study was determined by power analysis using the G*Power calculator (Universität Düsseldorf) for F-tests of one-way ANOVA by setting type I error at 5% (alpha = 0.05); power was kept at 0.8, and the number of treatment groups at 5. The effect size f was calculated as 0.707. This number was used to determine total sample size of 30 with 6 mice per treatment group (37). Six- to 7-week-old female BALB/C athymic nude mice (*nu/nu*; Charles River Laboratories) were implanted subcutaneously with 0.5-mg (60-day release), 17β-estradiol pellets (Innovative Research of America) on the upper dorsal side between the ear and shoulder to support growth of BT474 xenografts, which, in addition to HER2 overexpression, also express the estrogen receptor; a trocar needle was used. On the following day, 10^7 BT474 cells in 100-μL of PBS-Matrigel (1:1; BD Biosciences) were subcutaneously injected into mammary fat pad number 9. Tumor size was monitored by caliper at 2-day intervals, and tumor volume was calculated (tumor width^2 × its length/2). After the tumors reached a volume of >150 mm^3, mice were randomly assigned into groups (see Results). EVs (2×10^9) in 100-μL PBS were injected intraperitoneally (i.p.) per mouse per dose. Controls received an equal amount of PBS. The administration schedule, based on our previous PK/PD studies of the CNOB/HChrR6 regimen (7), is provided in the Results section.

Data and statistical analysis

Data were analyzed by the Prism software (GraphPad Inc.). Statistics were determined using Student *t* test; *P* values of less than 0.05 were considered statistically significant. The experimental data of each treatment group overtime were further analyzed by slope of linear regression and *t* test (Supplementary Materials and Methods).

Results

CNOB/ChrR6 treatment is effective *in vitro* against HER2$^+$ human breast cancer cells

The CNOB/ChrR6 prodrug approach is effective in killing several different cancer cell lines (3), but its effect on HER2$^+$ breast cancer cells was not examined. The regimen proved highly effective ($P < 0.001$; Fig. 1) in killing human breast cancer cells regardless of whether they are essentially HER2-negative (MCF7, 4.7-ng HER2 receptor/mg) or strongly positive (BT474, 530-ng HER2 receptor/mg; ref. 16), including a HER2$^+$ trastuzumab-resistant cell line (BT474/HER-Res). (Note, that for narrative convenience, the MCF7 cells will be referred to as HER2-negative from here on.)

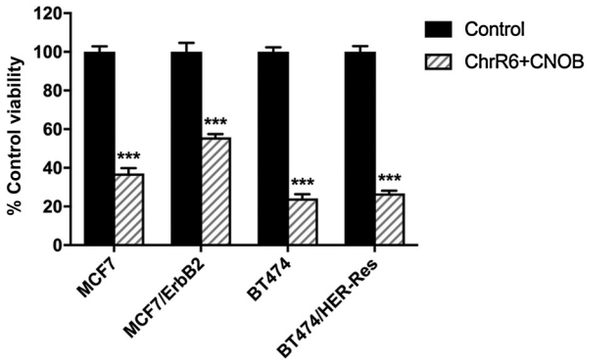

Figure 1.

Residual survival of cells after CNOB (15 μmol/L) and ChrR6 (50 μg/mL) treatment (for 24 hours) *in vitro.* Cell viability was determined by MTT assay. Data are presented as percent survival (hashed bar) compared with untreated controls (solid dark bar) of the corresponding cells. MCF7 cells express low and BT474 cells high levels of the HER2 ligand (see text). HER2-overexpressing counterpart of MCF7 cells ("MCF7/ErbB2") were included, as were trastuzumab-resistant BT474 cells ("BT474/HER2-Res"). ***, $P < 0.001$ as compared with untreated control of the corresponding cell line.

HER2-targeting EVs

To enable EVs to target HER2 receptors, we constructed the plasmid pEVC1C2HER. It encodes a chimeric protein, we have termed EVHB (Fig. 2A; Supplementary Fig. S1; GenBank accession no. MG838737), consisting of (i) lactadherin leader sequence (LS) for EVHB migration to the EV surface; (ii) high-affinity anti-HER2 scFv antibody (ML39; (K(d) = 10^{-9} mol/L; ref. 33) to target the HER2 receptor, connected through a flexible linker to (iii) lactadherin C1–C2 domains, which bind to EVs by interacting with their surface phosphatidylserine (38); and (iv) His-tag, for purification. Supplementary Fig. S1 shows the amino acid composition of EVHB, indicating a calculated molecular weight of 68 kDa. HEK293 cells were transfected with pEVC1C2HER, and the cell-released EVs were isolated; they presented a uniform peak in NanoSight analysis (average size, ca. 30–100 nm; Fig. 2B); TEM analysis showed a similar size range (Supplementary Fig. S2). The EVs were positive for three EV-specific proteins (39), CD63, CD81, and lactadherin (Supplementary Fig. S3). (293 FT EVs gave very similar results.)

Equal protein amounts of EV- or whole cell-lysates were analyzed by Western blotting; the expected 68-kDa band was seen, which was more intense for the EVs (Fig. 2C); the band was not found in extracts of nontransfected cells or their EVs. Unlike the finding of Hung and Leonard (40), EVHB escaped degradation by endosomal proteases; the possible reason for this difference is considered in the Discussion. The predicted three-dimensional structure of EVHB (Fig. 2D) is further elucidated in a video (Supplementary Video 1), showing rotation of its structure along two axes: ML39 with its heavy- and light-chain sequences is exposed outward, is joined to LS, and C1 and C2 domains are below it, orientated in opposite directions. This is consistent with the propensity of EVHB to bind to the EVs and display ML39.

We tested two methods to generate directed-EVs, one by obtaining them from pEVC1C2HER-transfected HEK293 cells, and the other, by first generating naïve EVs from nontransfected HEK293 cells and incubating them with pure EVHB. ELISA tests showed that the latter possessed 10-fold greater binding capability to the HER2 receptor than the former ("Reconstitution" vs. "Transfection" EVs; Fig. 3A and B). This is likely because the transfected cells transported less EVHB to the EV surface than the

Published OnlineFirst February 26, 2018; DOI: 10.1158/1535-7163.MCT-17-0827

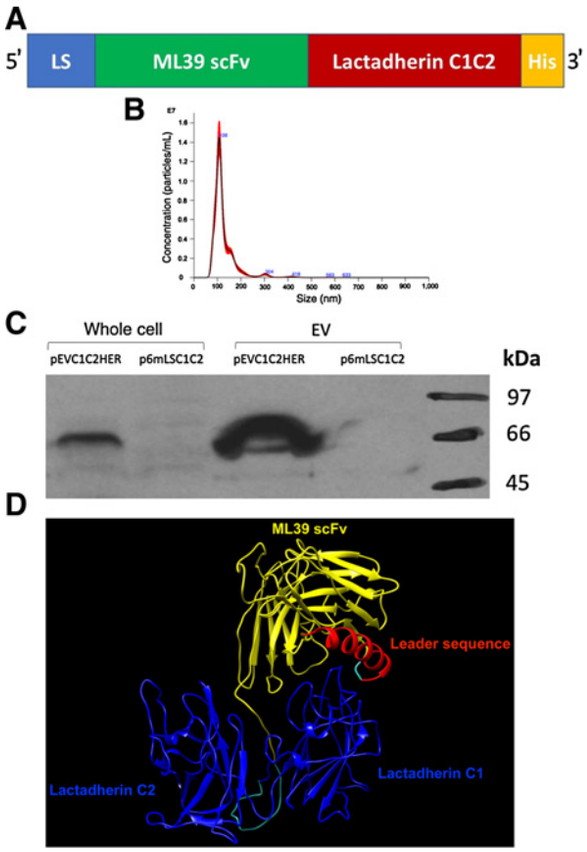

Figure 2.

HER2 receptor targeting ML39 chimeric protein (EVHB) and EV NanoSight analysis. **A,** Schematic of EVHB: LS (blue), lactadherin leader sequence for export of EVHB across the membrane; ML39 scFv (green), high-affinity (Kd = 10^{-9} mol/L) HER2-targeting moiety; lactadherin C1C2 domains (red), which enable EVHB to bind to the EV surface; His (orange), His-tag for purification; the predicted molecular weight of EVHB is 68 kDA (Supplementary Fig. S1). **B,** EV NanoSight analysis. **C,** Western blots. Protein extracts of whole cells of HEK293 cells transfected with pEVC1C2HER plasmid or EVs generated by them; cells transfected with the empty plasmid (p6mLSC1C2) were used as control; the 68 kDa band is seen only in the transfected cells and EVs generated from them. **D,** Predicted protein structure of EVHB. Color scheme: yellow, scFv antibody; red, leader sequence; blue, C1C2 domains.

locations available for its binding, and that greater binding saturation occurs when EVHB is externally added. This is illustrated in Fig. 3B ("Transfection" vs. "Reconstitution"). As all subsequent work used such "reconstituted" EVs, the term "directed" will denote these EVs.

We next compared relative binding of directed-EVs to HER2-overexpressing BT474- and HER2-negative MCF7 cells. The CFSE-labeled EVs were added to the cells. Fluorescent and phase contrast microscopic images of corresponding regions (Fig. 3C) showed that directed-EVs bound to BT474, but not to MCF7 cells. Treatment with PBS generated no signal. Not all BT474 cells evidently bound to the EVs, possibly because not all of them express this ligand to the same extent; that HER2 receptor density varies in $HER2^+$ cells has been reported (41). Given that MCHB has an excellent bystander effect, not all tumor cells need to receive HChR6 mRNA, and thus the lack of binding of EVs to all the cells would not necessarily hamper effective therapy.

We also used flow cytometry to determine the binding of EVs to $HER2^+$ cells. As already mentioned, because BT474 cells tended to form clumps, the $HER2^+$ cells used were SKBR3; these were treated with directed PKH26-labeled EVs. Three-way binding comparisons were made: SKBR3 or MCF7 cells alone; or a 50:50 mixture of the two. We arbitrarily assigned the fluorescence intensity shift generated by SKBR3 cells a value of 1 (Fig. 3D). In contrast, MCF7 cells generated a shift of 0.17. Thus, the directed-EVs exhibit a marked preference for binding to the $HER2^+$ cells. The shift exhibited by the mixture was 0.63, indicating that the concomitant presence of MCF7 cells did not interfere with the binding of directed-EVs to SKRB3 cells, a beneficial outcome, as HER2-overexpressing tumors also contain HER2-negative cells.

Loading of EVs with mRNA, its EV-mediated delivery specifically to $HER2^+$ cells, and to implanted tumors in mice

Loading EVs with exogenous mRNA that remains functional has not been accomplished (40). We attempted electroporation for this purpose. Nonelectroporated EVs contained more mRNA than the electroporated (100–400 V) ones, suggesting that the mRNA remained adhered to the surface of EVs, and was not internalized. Our electroporation method did succeed in loading the EVs with GAPDH siRNA (Supplementary Fig. S4), in agreement with previous reports (42), indicating that our technique was sound.

We developed a new method for inserting mRNA into the EVs. A special plasmid was constructed (Fig. 4A) using the "zipcode" technology (43) and the SBI XPort plasmid. Two tandem copies of the EV-loading zipcode sequence (5′-ACCCTGCCGCCTGGACTCCGCCTGT-3′) were inserted at the 3′ UTR of the *HchrR6* gene under the control of the constitutive MSCV promoter. This plasmid, named 'pXPort/HChrR6 mRNA', was used for transient transfection of 293FT cells. 4 days after transfection, the EVs were isolated from conditioned medium, and the HChrR6 mRNA was quantified; the Ct value is shown in Fig. 4B; it corresponds to 2×10^{-4} mRNA copy/EV.

The loaded EVs were incubated with EVHB, generating directed and loaded, EXO-DEPTs. These were tested for their ability to deliver HChrR6 mRNA to BT474 cells. The cells were incubated overnight with EXO-DEPTs, or as control, with naïve but loaded EVs (8×10^8/well). Successful transfer of HChrR6 mRNA to the recipient cells would enable them to activate CNOB. This was assessed by determining MCHB generation (monitored by its fluorescence) following CNOB addition. Cells treated with EXO-DEPTs—but not with the naïve-loaded EVs—converted CNOB into MCHB (Fig. 4C; $P < 0.01$). Actinomycin D (transcriptional inhibitor) did not affect this, but cyclohexamide (protein synthesis inhibitor) eliminated CNOB conversion (Fig. 4D; $P < 0.001$). Thus, it was functional mRNA that was transferred by the EXO-DEPT EVs, and for EVs to be able to do so, they needed to be directed.

We next tested the effect of EXO-DEPTs along with CNOB on orthotopically implanted BT474 tumors in athymic mice; the treatment schedule (Fig. 4E) was guided by our previous PK/PD studies. The half-life of MCHB in plasma is 8.3 hours (7), indicating that administration of the regimen at 24-hour interval (or longer) would allow adequate clearance of the drug from plasma and avoid systemic toxicity. After measurable

Published OnlineFirst February 26, 2018; DOI: 10.1158/1535-7163.MCT-17-0827

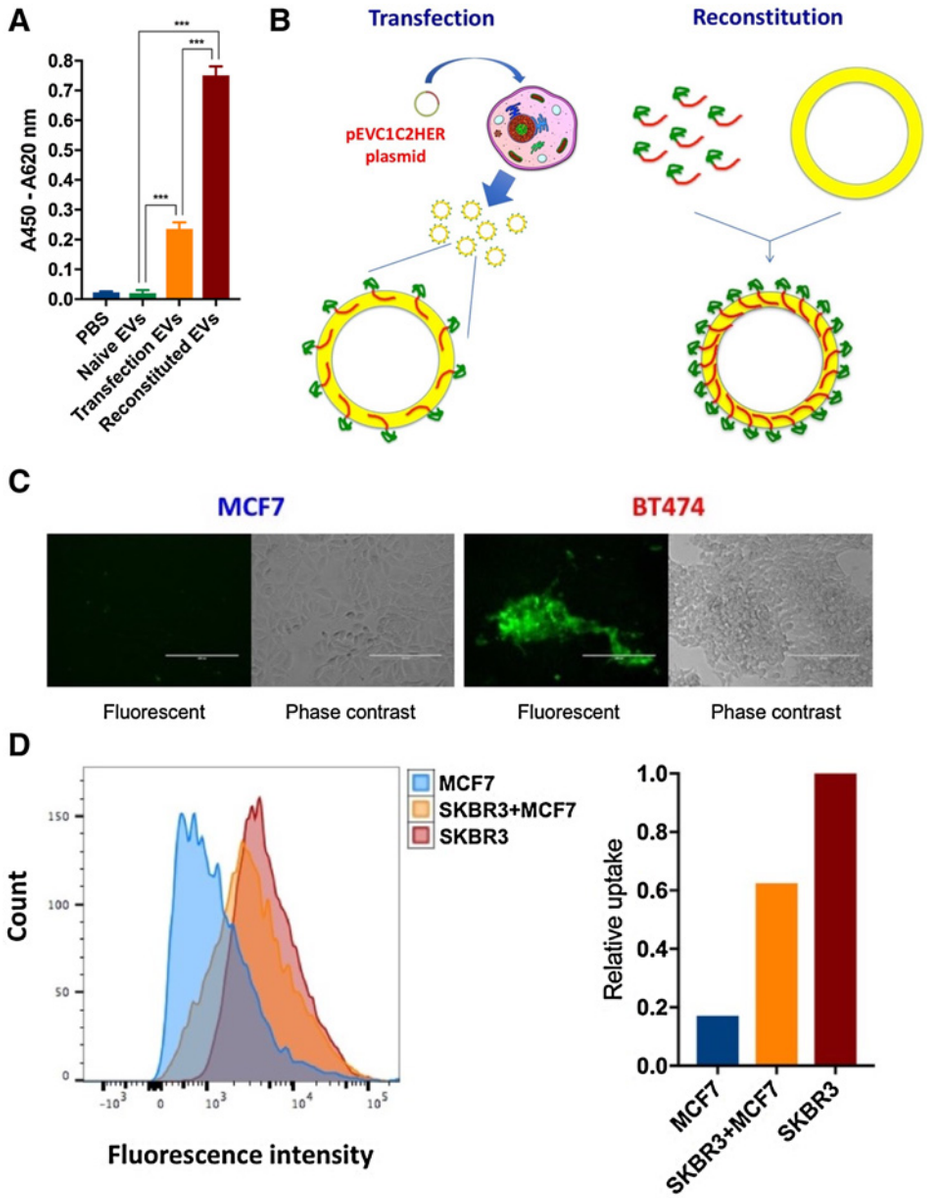

Figure 3.
Specificity of directed-EV (displaying EVHB) binding to HER2 receptor. **A,** ELISA detection of this activity: Orange bar, EVs obtained from pEVC1C2HER plasmid-transfected HEK293 cells; dark brown bar, EVs obtained from nontransfected HEK293 cells incubated with pure EVHB—these show greater binding capability (see text for details). No signal resulted when naïve EVs (isolated from nontransfected HEK293 cells not incubated with EVHB), or PBS. Bars, average value ± SD ($n = 3$). ***, $P < 0.001$ as determined by the t test between groups as indicated. **B,** Schematic representation of EVHB display by EVs: "Transfection" shows EVs from HEK 293 cells transfected with pEVC1C2HER plasmid; "Reconstitution" indicates EVs obtained from nontransfected cells after incubation with pure EVHB. Yellow circles represent EVs, and red squiggles with green heads represent EVHB; **C,** Visualization of directed-EV binding specifically to HER2$^+$ cells. Representative fluorescent and phase contrast images of corresponding regions are shown: CFSE-labeled (green) directed-EVs bind to BT474 cells and not to MCF7 cells. **D,** Directed-EV binding to cells as determined by flow cytometry. Left, Fluorescence shift caused by the indicated cell types (or mixture). The shift due to SKBR3 cells is arbitrarily assigned a value of 1 (see Results). Right, Quantification of the relative shifts based on the data of the left plot—binding is specific to HER2$^+$ cells.

implanted tumors in mice were detected, the mice were randomly allocated into 5 treatment groups ($n = 6$): untreated; loaded EVs only; CNOB only; undirected loaded EVs + CNOB; and EXO-DEPTs + CNOB. The treatment was started with intraperitoneal injection of 2×10^9 EVs and, 24 hours later, of intravenous (i.v.) injection of CNOB (3.3 mg/kg in saline); corresponding controls received PBS (instead of EVs) or saline (instead of CNOB). Further doses (in the same amounts) were given as shown in Fig. 4E.

Tumor volume was recorded twice a week; each data point in Fig. 4F represents average value for a given treatment group. Slopes of linear regression, which represent tumor growth rate of individual mice, were calculated and are shown in the box-and-whisker plot (Fig. 4G). Mice receiving EXO-DEPTs + CNOB began to show statistically significant ($P < 0.01$) difference in tumor volumes versus the controls on day 11; this became more marked ($P < 0.001$) as the experiment progressed (Fig. 4F). Note that this group shows near-complete arrest of tumor growth. Tumor development was also mitigated in the loaded, undirected EVs + CNOB group, as was expected from the fact, referred to above, that EVs can extravasate through vessel fenestrations of tumors; lack of effective lymphatic drainage in solid tumors further promotes this "Enhanced permeability retention (EPR)" effect. That the EXO-DEPTs were twice as effective ($P < 0.01$ compared with the nondirected EV group) in suppressing tumor growth underscores the success of our targeting strategy. There was no significant difference among untreated, EV-only, and CNOB-only groups. The experiment was stopped because the tumors in control groups had begun to exceed the volume allowed by the animal protocol. A prior experiment in which only two groups were used—EXO-DEPTs plus CNOB-treated and untreated control ($n = 5$)—gave very similar results.

Published OnlineFirst February 26, 2018; DOI: 10.1158/1535-7163.MCT-17-0827

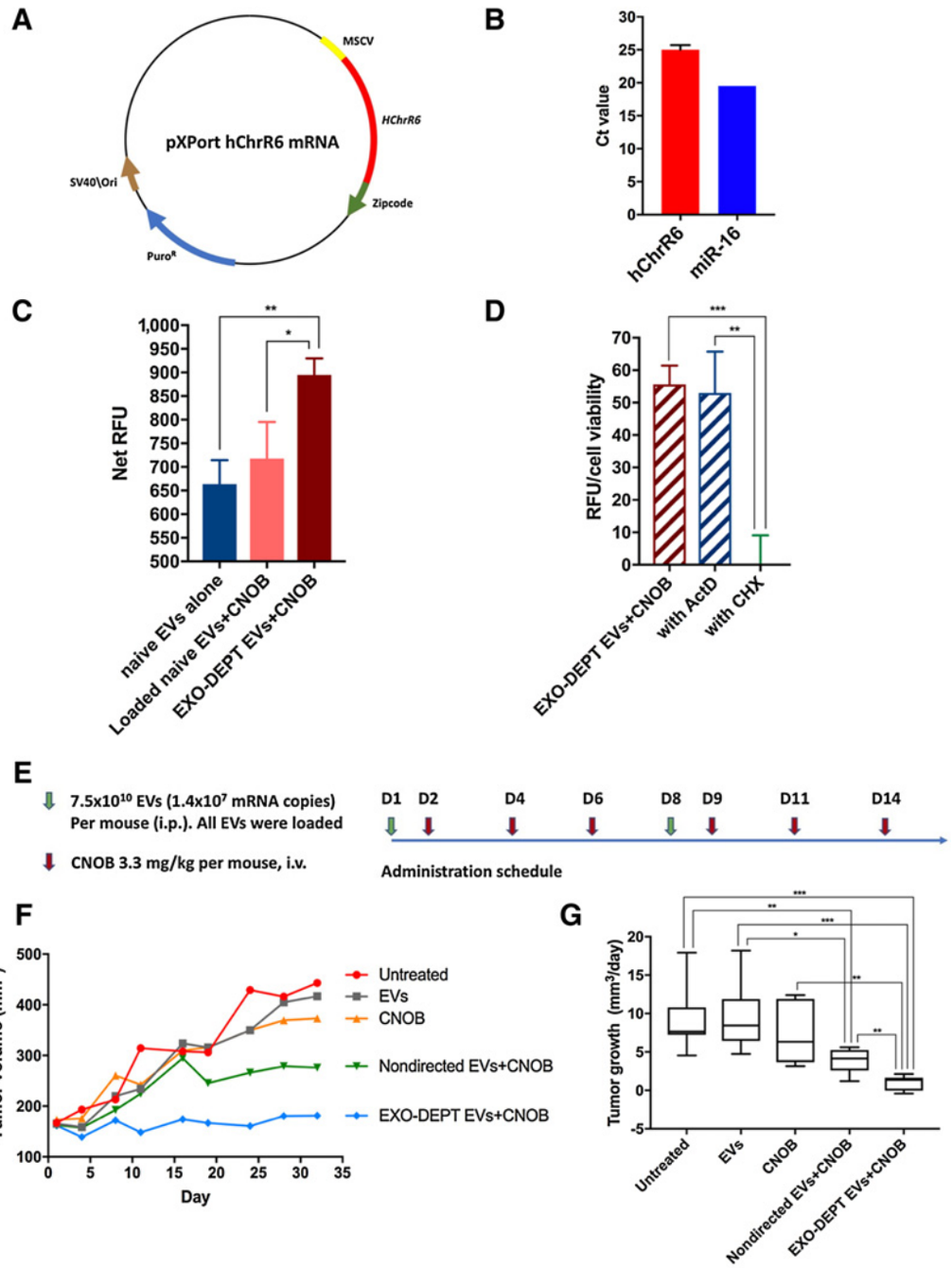

Figure 4.

Loading of EVs with HChrR6 mRNA and EXO-DEPT functionality *in vitro* and *in vivo*. **A,** Design of XPort/HChrR6 plasmid showing key features involved in mRNA packaging into EVs; see text for details. **B,** qPCR results showing successful loading of EVs with HChrR6 mRNA. Endogenous EV miR-16 level was determined as control. (The Ct value of mRNA corresponds to 2×10^{-4} copy/EV.). **C,** *In vitro* effectiveness of EXO-DEPT EVs. BT474 cells (3×10^4) treated with 8×10^8 EXO-DEPT EVs generated MCHB fluorescence upon CNOB treatment (dark brown bar); naïve EVs alone (dark blue bar) or loaded but nondirected EVs (not displaying EVHB; orange bar) show only background fluorescence upon CNOB treatment. **D,** MCHB fluorescence normalized to cell viability. BT474 cells treated with EXO-DEPT EVs and CNOB generate MCHB fluorescence (hashed brown bar), which is not affected by the presence of actinomycin D (hashed blue bar) but is eliminated in the presence of cyclohexamide (CHX). See text for further details. Bars represent average value ± SD ($n = 3$). ***, $P < 0.001$; **, $P < 0.01$ as compared between groups as indicated. **E,** Administration schedule of EVs and CNOB for *in vivo* test of the effectiveness of EXO-DEPT EVs. *Nu/nu* mice implanted with orthotopic BT474 tumors were used (the number of EVs administered delivered 4×10^5 copies of the HChrR6 mRNA per injection; CNOB per injection was 3.3 mg/kg). **F,** Plot of average tumor volume recorded twice a week for the indicated treatment groups. **G,** Rate of tumor growth calculated from slopes of linear regression shown in box-and-whisker plot for each treatment group. Statistical analysis of linear regression slopes between groups was performed by two-samples, two-sided *t* test, and confirmed by Tukey honest significance difference test as *post hoc*. ***, $P < 0.001$; **, $P < 0.01$; *, $P < 0.05$ as compared between groups as indicated. Further statistical analysis is provided in Supplementary Materials and Methods.

Published OnlineFirst February 26, 2018; DOI: 10.1158/1535-7163.MCT-17-0827

Discussion

EVs are receiving increasing attention as vehicles for safe delivery of drugs and exogenous biomolecules, such as silencing small RNAs, to tissues for therapeutic purposes (23). As directed delivery of such agents to specific tissues has obvious advantages, successful attempts have been made to fuse ligands to EV surface that target specific receptors. Examples include delivery of doxorubicin by αv itegrins-targeted EVs to tumors (44); use of epidermal growth factor receptor (EGFR)-targeted EVs (45, 46) to transport molecules, such as let-7ainordertodeliverlet-7a (let7a), to breast cancer in mice; and cationized pullulan-treated EVs to target asialoglycoprotein receptors specifically expressed by hepatocytes (47). Our specific targeting of HER2 receptor by EVs decorated with EVHB represents further advance in this direction. ELISA analysis showed that for these EVs to bind the HER2 receptor, they needed to be directed, i.e., display EVHB; and both microscopic and flow-cytometry approaches confirmed that the directed EVs bind selectively to $HER2^+$ cells. Hung and Leonard (40) found that peptides displayed on their EVs were degraded by endosomal proteases, unless a glycosylation motif was incorporated in the conjugate. The reason why, in contrast, successful display by our EVs of EVHB did not require glycosylation is not known. It may, however, be related to the fact that in the EVs of Hung and Leonard, the displayed peptides were conjugated to the EV-associated transmembrane protein Lamp2b ("lysosomal associated membrane protein-2"), in contrast to our use of the C1–C2 domains for this purpose. Lamp2b, being lysosome associated, may have directed the conjugate to the autophagy pathway (48), leading to lysosomal degradation. It is pertinent in this regard that our own initial attempts to use Lamp2b protein to display the HER2-targeting ligand did not result in directed- EVs.

A major advance reported here concerns the construction of EXO-DEPTs that not only specifically target the $HER2^+$ cells but are also capable of delivering to them functional HChrR6 mRNA. Insertion of foreign mRNA into EVs has been a challenge. Electroporation has not succeeded. Utilization of a bacteriophage protein bridge between EVs and mRNA did result in successful loading; but this mRNA, when delivered by the EVs to recipient cells, was nonfunctional (40). Our EXO-DEPTs, however, converted BT474 cells into CNOB activating entities, resulting in MCHB generation and cell killing. This effect was not inhibited by actinomycin D, showing that the ingredient transferred by the EVs was indeed HChrR6 mRNA. EXO-DEPTs also effectively delivered the HChrR6 mRNA *in vivo*: when administered along with CNOB, they caused near-complete arrest of the growth of implanted orthotopic HER2-overexpressing breast cancer tumors in athymic mice. To our knowledge, this is the first time that EV-mediated exogenous mRNA delivery has been accomplished to therapeutic advantage. Foreign miRNA has been successfully delivered before using EVs, as noted above. Another example is the EnGeneIC Delivery Vehicle (EDV)-mediated EGFR-targeted delivery of miR-16–based mimics to successfully treat malignant pleural mesothelioma (49). This sheds further positive light on the possibility of successful clinical use of EVs.

While tumor growth was arrested, the tumors were not eliminated, and studies are in progress to further improve the EXO-DEPT/CNOB regimen. Measures under investigation include increased HChrR6 mRNA loading into the EVs, and dosage/regimen optimization of EXO-DEPTs and CNOB. HChrR6 is also effective in activating another prodrug, CB1954 (5), for which a safe dosage has been established in clinical trials (50). The effect of combined therapy with CNOB and CB1954 is also therefore being explored. In addition, we are experimenting with immunocompetent mice to combine EXO-DEPT/prodrug and immune-based antitumor effectors.

What effect the indigenous content of EVs might have on recipient cells may be of concern, but this is mitigated by the finding (51) that the administration of HEK293 EVs resulted in minimal immunogenicity and toxicity *in vivo*. Nevertheless, we are attempting to decrease the EXO-DEPTs needed for effective treatment, as it would eliminate the need for administering them to the patients in large quantities.

EVs can cross the blood–brain barrier (52–55). Metastasis to the brain is a common complication of HER2-overexpressing breast cancer (56), and whether the EXO-DEPT/prodrug therapy can be effective in addressing this complication is also being investigated.

We note that the EVHB-based approach is generic. ML39 in EVHB can be replaced by other targeting ligands to make directed-EVs for delivering desired biomolecules/drugs to any disease in which a marker is overexpressed. Examples of other receptors overexpressed in cancers are PSMA, bombasin, folate, transferrin, and sigma (57–60). This approach can also permit construction of dual function EVs that not only target the HER2 receptor but can also be visualized. This can be done by treating naïve EVs with EVHB plus C1–C2–conjugated reporters, e.g, GLuc, mCherry, or eGFP. The possibility of adding additional functionality can further enhance the EV-based therapies (61).

To conclude, the EXO-DEPT/CNOB regimen is effective in specifically targeting and arresting tumor growth *in vivo*. Our previous studies have demonstrated that patient-specific exosomes derived from dendritic cells can be reliably produced under GMP for clinical use (21, 62–65). This favorably illustrates the potential feasibility of the EXO-DEPT approach for therapeutic development.

Disclosure of Potential Conflicts of Interest

A. Delcayre is a partner at ExoThera and has ownership interest (including patents) in the same. No potential conflicts of interest were disclosed by the other authors.

Disclaimer

The content is solely the responsibility of the authors and does not necessarily represent the official views of the NIH.

Authors' Contributions

Conception and design: J.-H. Wang, D.O. Frimannsson, A. Delcayre, T.J. Antes, S.S. Jeffrey, M.D. Pegram, A.C. Matin

Development of methodology: J.-H. Wang, A.V. Forterre, D.O. Frimannsson, A. Delcayre, T.J. Antes, B. Efron, M.D. Pegram, A.C. Matin

Acquisition of data (provided animals, acquired and managed patients, provided facilities, etc.): J.-H. Wang, A.V. Forterre, D.O. Frimannsson, M.D. Pegram, A.C. Matin

Analysis and interpretation of data (e.g., statistical analysis, biostatistics, computational analysis): J.-H. Wang, D.O. Frimannsson, A. Delcayre, T.J. Antes, M.D. Pegram, A.C. Matin

Writing, review, and/or revision of the manuscript: J.-H. Wang, D.O. Frimannsson, A. Delcayre, T.J. Antes, M.D. Pegram, A.C. Matin

Administrative, technical, or material support (i.e., reporting or organizing data, constructing databases): J.-H. Wang, J. Zhao, A.C. Matin

Study supervision: A.C. Matin

Other (coordination between principals on the project): A.C. Matin

Acknowledgments

Research reported in this publication was supported by the National Center for Advancing Translational Sciences of the NIH under Award Number UH3TR000902 to A.C. Matin; J. Zhao was supported in part by the First Affiliated Hospital of Guangzhou Medical University. We gratefully acknowledge the valuable feedback provided by NIH scientists, Drs. Danilo Tagle, Lillian Kuo, Tania Lombo Rodriguez, and Kayla Valdes.

The costs of publication of this article were defrayed in part by the payment of page charges. This article must therefore be hereby marked *advertisement* in accordance with 18 U.S.C. Section 1734 solely to indicate this fact.

Received August 28, 2017; revised December 29, 2017; accepted February 9, 2018; published first February 26, 2018.

References

1. Padma VV. An overview of targeted cancer therapy. Biomedicine (Taipei) 2015;5:19.
2. Williams EM, Little RF, Mowday AM, Rich MH, Chan-Hyams JV, Copp JN, et al. Nitroreductase gene-directed enzyme prodrug therapy: insights and advances toward clinical utility. Biochem J 2015;471: 131–53.
3. Thorne SH, Barak Y, Liang W, Bachmann MH, Rao J, Contag CH, et al. CNOB/ChrR6, a new prodrug enzyme cancer chemotherapy. Mol Cancer Ther 2009;8:333–41.
4. Barak Y, Ackerley DF, Dodge CJ, Banwari L, Alex C, Francis AJ, et al. Analysis of novel soluble chromate and uranyl reductases and generation of an improved enzyme by directed evolution. Appl Environ Microbiol 2006; 72:7074–82.
5. Barak Y, Thorne SH, Ackerley DF, Lynch SV, Contag CH, Matin A. New enzyme for reductive cancer chemotherapy, YieF, and its improvement by directed evolution. Mol Cancer Ther 2006;5:97–103.
6. Eswaramoorthy S, Poulain S, Hienerwadel R, Bremond N, Sylvester MD, Zhang YB, et al. Crystal structure of ChrR–a quinone reductase with the capacity to reduce chromate. PLoS One 2012;7:e36017.
7. Wang JH, Endsley AN, Green CE, Matin AC. Utilizing native fluorescence imaging, modeling and simulation to examine pharmacokinetics and therapeutic regimen of a novel anticancer prodrug. BMC Cancer 2016; 16:524.
8. Lelekakis M, Moseley JM, Martin TJ, Hards D, Williams E, Ho P, et al. A novel orthotopic model of breast cancer metastasis to bone. Clin Exp Metastasis 1999;17:163–70.
9. Franklin MC, Carey KD, Vajdos FF, Leahy DJ, de Vos AM, Sliwkowski MX. Insights into ErbB signaling from the structure of the ErbB2-pertuzumab complex. Cancer Cell 2004;5:317–28.
10. Yarden Y, Sliwkowski MX. Untangling the ErbB signalling network. Nat Rev Mol Cell Biol 2001;2:127–37.
11. Slamon DJ, Clark GM, Wong SG, Levin WJ, Ullrich A, McGuire WL, et al. Human breast cancer: correlation of relapse and survival with amplification of the HER-2/neu oncogene. Science 1987;235:177–82.
12. Slamon DJ, Godolphin W, Jones LA, Holt JA, Wong SG, Keith DE, et al. Studies of the HER-2/neu proto-oncogene in human breast and ovarian cancer. Science 1989;244:707–12.
13. Slamon D, Eiermann W, Robert N, Pienkowski T, Martin M, Press M, et al. Adjuvant trastuzumab in HER2-positive breast cancer. N Engl J Med 2011;365:1273–83.
14. Romond EH, Perez EA, Bryant J, Suman VJ, Geyer CE Jr, Davidson NE, et al. Trastuzumab plus adjuvant chemotherapy for operable HER2-positive breast cancer. N Engl J Med 2005;353:1673–84.
15. Pegram M, Hsu S, Lewis G, Pietras R, Beryt M, Sliwkowski M, et al. Inhibitory effects of combinations of HER-2/neu antibody and chemotherapeutic agents used for treatment of human breast cancers. Oncogene 1999;18:2241–51.
16. Konecny GE, Pegram MD, Venkatesan N, Finn R, Yang G, Rahmeh M, et al. Activity of the dual kinase inhibitor lapatinib (GW572016) against HER-2-overexpressing and trastuzumab-treated breast cancer cells. Cancer Res 2006;66:1630–9.
17. Geyer CE, Forster J, Lindquist D, Chan S, Romieu CG, Pienkowski T, et al. Lapatinib plus capecitabine for HER2-positive advanced breast cancer. N Engl J Med 2006;355:2733–43.
18. Duarte S, Carle G, Faneca H, de Lima MC, Pierrefite-Carle V. Suicide gene therapy in cancer: where do we stand now? Cancer Lett 2012; 324:160–70.
19. Bai L, Shao H, Wang H, Zhang Z, Su C, Dong L, et al. Effects of Mesenchymal stem cell-derived exosomes on experimental autoimmune uveitis. Sci Rep 2017;7:4323.
20. Colombo M, Raposo G, Thery C. Biogenesis, secretion, and intercellular interactions of exosomes and other extracellular vesicles. Annu Rev Cell Dev Biol 2014;30:255–89.
21. Delcayre A, Estelles A, Sperinde J, Roulon T, Paz P, Aguilar B, et al. Exosome Display technology: applications to the development of new diagnostics and therapeutics. Blood Cells Mol Dis 2005;35: 158–68.
22. El Andaloussi S, Lakhal S, Mager I, Wood MJ. Exosomes for targeted siRNA delivery across biological barriers. Adv Drug Deliv Rev 2013; 65:391–7.
23. Ha D, Yang N, Nadithe V. Exosomes as therapeutic drug carriers and delivery vehicles across biological membranes: current perspectives and future challenges. Acta Pharm Sin B 2016;6:287–96.
24. van den Boorn JG, Dassler J, Coch C, Schlee M, Hartmann G. Exosomes as nucleic acid nanocarriers. Adv Drug Deliv Rev 2013;65:331–5.
25. van den Boorn JG, Schlee M, Coch C, Hartmann G. SiRNA delivery with exosome nanoparticles. Nat Biotechnol 29:325–6.
26. Rainov NG. A phase III clinical evaluation of herpes simplex virus type 1 thymidine kinase and ganciclovir gene therapy as an adjuvant to surgical resection and radiation in adults with previously untreated glioblastoma multiforme. Hum Gene Ther 2000;11:2389–401.
27. Schenk E, Essand M, Bangma CH, GIANT FP6 Consortium, Barber C, Behr JP, et al. Clinical adenoviral gene therapy for prostate cancer. Hum Gene Ther 2010;21:807–13.
28. Onion D, Patel P, Pineda RG, James N, Mautner V. Antivector and tumor immune responses following adenovirus-directed enzyme prodrug therapy for the treatment of prostate cancer. Hum Gene Ther 2009;20:1249–58.
29. Patel P, Young JG, Mautner V, Ashdown D, Bonney S, Pineda RG, et al. A phase I/II clinical trial in localized prostate cancer of an adenovirus expressing nitroreductase with CB1954 [correction of CB1984]. Mol Ther 2009;17:1292–9.
30. Zabner J, Fasbender AJ, Moninger T, Poellinger KA, Welsh MJ. Cellular and molecular barriers to gene transfer by a cationic lipid. J Biol Chem 1995;270:18997–9007.
31. Zou S, Scarfo K, Nantz MH, Hecker JG. Lipid-mediated delivery of RNA is more efficient than delivery of DNA in non-dividing cells. Int J Pharm 2010;389:232–43.
32. Okumura K, Nakase M, Inui M, Nakamura S, Watanabe Y, Tagawa T. Bax mRNA therapy using cationic liposomes for human malignant melanoma. J Gene Med 2008;10:910–7.
33. Li X, Stuckert P, Bosch I, Marks JD, Marasco WA. Single-chain antibody-mediated gene delivery into ErbB2-positive human breast cancer cells. Cancer Gene Ther 2001;8:555–65.
34. Kanada M, Bachmann MH, Hardy JW, Frimannson DO, Bronsart L, Wang A, et al. Differential fates of biomolecules delivered to target cells via extracellular vesicles. Proc Natl Acad Sci U S A 2015;112: E1433–42.
35. Kelley LA, Mezulis S, Yates CM, Wass MN, Sternberg MJ. The Phyre2 web portal for protein modeling, prediction and analysis. Nat Protoc 2015;10:845–58.
36. Alvarez-Erviti L, Seow Y, Yin H, Betts C, Lakhal S, Wood MJ. Delivery of siRNA to the mouse brain by systemic injection of targeted exosomes. Nat Biotechnol 2011;29:341–5.
37. Charan J, Kantharia ND. How to calculate sample size in animal studies? J Pharmacol Pharmacother 2013;4:303–6.
38. Otzen DE, Blans K, Wang H, Gilbert GE, Rasmussen JT. Lactadherin binds to phosphatidylserine-containing vesicles in a two-step mechanism sensitive to vesicle size and composition. Biochim Biophys Acta 2012; 1818:1019–27.

Published OnlineFirst February 26, 2018; DOI: 10.1158/1535-7163.MCT-17-0827

39. Lotvall J, Hill AF, Hochberg F, Buzás EI, Di Vizio D, Gardiner C, et al. Minimal experimental requirements for definition of extracellular vesicles and their functions: a position statement from the International Society for Extracellular Vesicles. J Extracell Vesicles 2014;3:26913.
40. Hung ME, Leonard JN. A platform for actively loading cargo RNA to elucidate limiting steps in EV-mediated delivery. J Extracell Vesicles 2016;5:31027.
41. Hendriks BS, Klinz SG, Reynolds JG, Espelin CW, Gaddy DF, Wickham TJ. Impact of tumor HER2/ERBB2 expression level on HER2-targeted liposomal doxorubicin-mediated drug delivery: multiple low-affinity interactions lead to a threshold effect. Mol Cancer Ther 2013;12:1816–28.
42. Momen-Heravi F, Bala S, Bukong T, Szabo G. Exosome-mediated delivery of functionally active miRNA-155 inhibitor to macrophages. Nanomedicine 2014;10:1517–27.
43. Bolukbasi MF, Mizrak A, Ozdener GB, Madlener S, Ströbel T, Erkan EP, et al. miR-1289 and "Zipcode"-like sequence enrich mRNAs in microvesicles. Mol Ther Nucleic Acids 2012;1:e10.
44. Tian Y, Li S, Song J, Ji T, Zhu M, Anderson GJ, et al. A doxorubicin delivery platform using engineered natural membrane vesicle exosomes for targeted tumor therapy. Biomaterials 2014;35:2383–90.
45. Kooijmans SA, Aleza CG, Roffler SR, van Solinge WW, Vader P, Schiffelers RM. Display of GPI-anchored anti-EGFR nanobodies on extracellular vesicles promotes tumour cell targeting. J Extracell Vesicles 2016;5:31053.
46. Ohno S, Takanashi M, Sudo K, Ueda S, Ishikawa A, Matsuyama N, et al. Systemically injected exosomes targeted to EGFR deliver antitumor microRNA to breast cancer cells. Mol Ther 2013;21:185–91.
47. Tamura R, Uemoto S, Tabata Y. Augmented liver targeting of exosomes by surface modification with cationized pullulan. Acta Biomater 2017;57:274–84.
48. Morell C, Bort A, Vara-Ciruelos D, Ramos-Torres Á, Altamirano-Dimas M, Díaz-Laviada I, et al. Up-regulated expression of LAMP2 and autophagy activity during neuroendocrine differentiation of prostate cancer LNCaP cells. PLoS One 2016;11:e0162977.
49. Kao SC, Fulham M, Wong K, Cooper W, Brahmbhatt H, MacDiarmid J, et al. A significant metabolic and radiological response after a novel targeted MicroRNA-based treatment approach in malignant pleural mesothelioma. Am J Respir Crit Care Med 2015;191:1467–9.
50. Chung-Faye G, Palmer D, Anderson D, Clark J, Downes M, Baddeley J, et al. Virus-directed, enzyme prodrug therapy with nitroimidazole reductase: a phase I and pharmacokinetic study of its prodrug, CB1954. Clin Cancer Res 2001;7:2662–8.
51. Zhu X, Badawi M, Pomeroy S, Sutaria DS, Xie Z, Baek A, et al. Comprehensive toxicity and immunogenicity studies reveal minimal effects in mice following sustained dosing of extracellular vesicles derived from HEK293T cells. J Extracell Vesicles 2017;6:1324730.
52. Fruhbeis C, Frohlich D, Kramer-Albers EM. Emerging roles of exosomes in neuron-glia communication. Front Physiol 2012;3:119.
53. Kalani A, Tyagi A, Tyagi N. Exosomes: mediators of neurodegeneration, neuroprotection and therapeutics. Mol Neurobiol 2014;49:590–600.
54. Xin H, Li Y, Chopp M. Exosomes/miRNAs as mediating cell-based therapy of stroke. Front Cell Neurosci 2014;8:377.
55. Yang TZ, Martin P, Fogarty B, Brown A, Schurman K, Phipps R, et al. Exosome delivered anticancer drugs across the blood-brain barrier for brain cancer therapy in Danio Rerio. Pharm Res 2015;32:2003–14.
56. Stemmler HJ, Schmitt M, Willems A, Bernhard H, Harbeck N, Heinemann V. Ratio of trastuzumab levels in serum and cerebrospinal fluid is altered in HER2-positive breast cancer patients with brain metastases and impairment of blood-brain barrier. Anticancer Drugs 2007;18:23–8.
57. Reynolds AR, Moein Moghimi S, Hodivala-Dilke K. Nanoparticle-mediated gene delivery to tumour neovasculature. Trends Mol Med 2003;9:2–4.
58. Lu Y, Low PS. Immunotherapy of folate receptor-expressing tumors: review of recent advances and future prospects. J Control Release 2003;91:17–29.
59. Kasperzyk JL, Finn SP, Flavin R, Fiorentino M, Lis R, Hendrickson WK, et al. Prostate-specific membrane antigen protein expression in tumor tissue and risk of lethal prostate cancer. Cancer Epidemiol Biomarkers Prev 2013;22:2354–63.
60. Akhtar MJ, Ahamed M, Alhadlaq HA, Alrokayan SA, Kumar S. Targeted anticancer therapy: overexpressed receptors and nanotechnology. Clin Chim Acta 2014;436:78–92.
61. Jensen M, Berthold F. Targeting the neural cell adhesion molecule in cancer. Cancer Lett 2007;258:9–21.
62. Amin A, Dudek AZ, Logan TF, Lance RS, Holzbeierlein JM, Knox JJ, et al. Survival with AGS-003, an autologous dendritic cell-based immunotherapy, in combination with sunitinib in unfavorable risk patients with advanced renal cell carcinoma (RCC): Phase 2 study results. J Immunother Cancer 2015;3:14.
63. Figlin RA, Amin A, Dudek A, Logan T, Lance RS, Holzbeierlein JM, et al. Phase II study combining personalized dendritic cell (DC)-based therapy, AGS-003, with sunitinib in metastatic renal cell carcinoma (mRCC). J Clin Oncol 2012;30:348–50.
64. Jurisica I, Gamble AH, Tcherepanova IY, Williams WL, Plessinger D, Miesowicz F, et al. Identification of multifunctional cytotoxic T-cell subsets as immune correlates with clinical outcomes in a phase II study of AGS-003, an autologous dendritic cell-based therapy administered to patients with newly diagnosed, metastatic RCC. J Clin Oncol 2012;30:80–3.
65. Nicolette CA, Healey D, Tcherepanova I, Whelton P, Monesmith T, Coombs L, et al. Dendritic cells for active immunotherapy: optimizing design and manufacture in order to develop commercially and clinically viable products. Vaccine 2007;25 Suppl 2:B47–60.

Published OnlineFirst February 26, 2018; DOI: 10.1158/1535-7163.MCT-17-0827

Molecular Cancer Therapeutics

Anti-HER2 scFv-Directed Extracellular Vesicle-Mediated mRNA-Based Gene Delivery Inhibits Growth of HER2-Positive Human Breast Tumor Xenografts by Prodrug Activation

Jing-Hung Wang, Alexis V. Forterre, Jinjing Zhao, et al.

Mol Cancer Ther 2018;17:1133-1142. Published OnlineFirst February 26, 2018.